JACS
JOURNAL OF THE AMERICAN CHEMICAL SOCIETY
pubs.acs.org/JACS
Article

Unveiling the Potential of Ambient Air Annealing for Highly Efficient Inorganic $CsPbI_3$ Perovskite Solar Cells

Zafar Iqbal, Roberto Félix, Artem Musiienko, Jarla Thiesbrummel, Hans Köbler, Emilio Gutierrez-Partida, Thomas W. Gries, Elif Hüsam, Ahmed Saleh, Regan G. Wilks, Jiahuan Zhang, Martin Stolterfoht, Dieter Neher, Steve Albrecht, Marcus Bär, Antonio Abate,* and Qiong Wang*

Cite This: J. Am. Chem. Soc. 2024, 146, 4642−4651
Read Online
ACCESS | Metrics & More | Article Recommendations | Supporting Information

ABSTRACT: Here, we report a detailed surface analysis of dry- and ambient air-annealed $CsPbI_3$ films and their subsequent modified interfaces in perovskite solar cells. We revealed that annealing in ambient air does not adversely affect the optoelectronic properties of the semiconducting film; instead, ambient air-annealed samples undergo a surface modification, causing an enhancement of band bending, as determined by hard X-ray photoelectron spectroscopy measurements. We observe interface charge carrier dynamics changes, improving the charge carrier extraction in $CsPbI_3$ perovskite solar cells. Optical spectroscopic measurements show that trap state density is decreased due to ambient air annealing. As a result, air-annealed $CsPbI_3$-based $n-i-p$ structure devices achieved a 19.8% power conversion efficiency with a 1.23 V open circuit voltage.

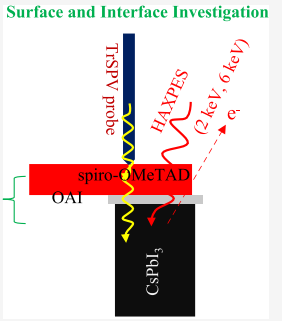

1. INTRODUCTION

Metal halide perovskites (MHPs) have emerged as promising candidates in the optoelectronic industry owing to their unique optoelectronic properties such as tunable bandgap,[1−3] long charge carrier diffusion length,[4,5] high defect tolerance,[6,7] and high light absorption coefficient.[8,9] Since Miyasaka et al. in 2009 first reported the use of halide perovskites as light absorbers in solar cells reaching power conversion efficiencies (PCE) of 3.8%,[10] the PCE of corresponding devices has climbed to 26.1% for single junction solar cells today,[11] surpassing the record PCE set by contemporary photovoltaic thin-film technologies based on e.g., copper indium gallium selenide (CIGS) (23.4%), CdTe (22.1%), and organic (19.2%) light absorbers,[12,13] thus now approaching the detailed balance limit (~33%).[14−16] However, the long-term stability of halide perovskite solar cells (PSC) lags significantly because of the presence of volatile organic cations, such as methylammonium (MA^+), in the crystal structure and its sensitivity to high temperature and moisture.[17−19] Replacing the volatile organic cations with Cs^+, i.e., the development of inorganic halide perovskites expressed as $CsPbX_3$ (where X stands for halide, such as chloride, bromide, and iodide) is hence one mitigation strategy that is studied in the research field.[20] Inorganic halide perovskites exhibit high thermal stability at temperatures exceeding 300 °C.[21] Among the $CsPbX_3$ compounds, $CsPbI_3$ has the lowest optical bandgap, E_g (~1.7 eV),[22] making it an excellent light absorber candidate for the top cell in a tandem structure with silicon or a narrow E_g perovskite as the bottom cell light absorber.[23] Besides, inorganic halide perovskites promise to outperform their organic−inorganic hybrid counterparts in terms of long-term stability at elevated operating temperatures (reaching 85 °C).[24] For these reasons, $CsPbI_3$ has received significant attention in the perovskite photovoltaic community.[25]

$CsPbI_3$ undergoes crystal phase transitions, transforming from a cubic (α) phase to a tetragonal (β) phase, to an orthorhombic (γ) phase as its temperature decreases from above 300 °C to room temperature.[26] Due to the low tolerance factor in $CsPbI_3$, maintaining phase stability at room temperature requires special attention.[27] Furthermore, obtaining pinhole-free $CsPbI_3$ films with low defect densities remained challenging.[28,29] However, controlling the nucleation and crystallization of $CsPbI_3$ has been suggested to overcome this obstacle, with many efforts made to this end.[30−34] In addressing this challenge, Wang et al. introduced dimethylammonium iodide (DMAI) in the precursor of $CsPbI_3$, which resulted in a stabilized β-phase with an E_g of 1.68 eV.[35] Further, the postpassivation with long-chain organic halides, such as choline iodide (CHI) and large cation halide, phenyltrimethylammonium chloride (PTACl), increases the PCE of resulting devices up to 19%.[35,36] The role of DMAI, whether it remains in the final crystal structure of $CsPbI_3$ has been investigated.[21,29,36] For example, it has been reported that

Received: October 20, 2023
Revised: January 9, 2024
Accepted: January 10, 2024
Published: February 9, 2024

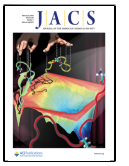

https://doi.org/10.1021/jacs.3c11711
J. Am. Chem. Soc. 2024, 146, 4642−4651

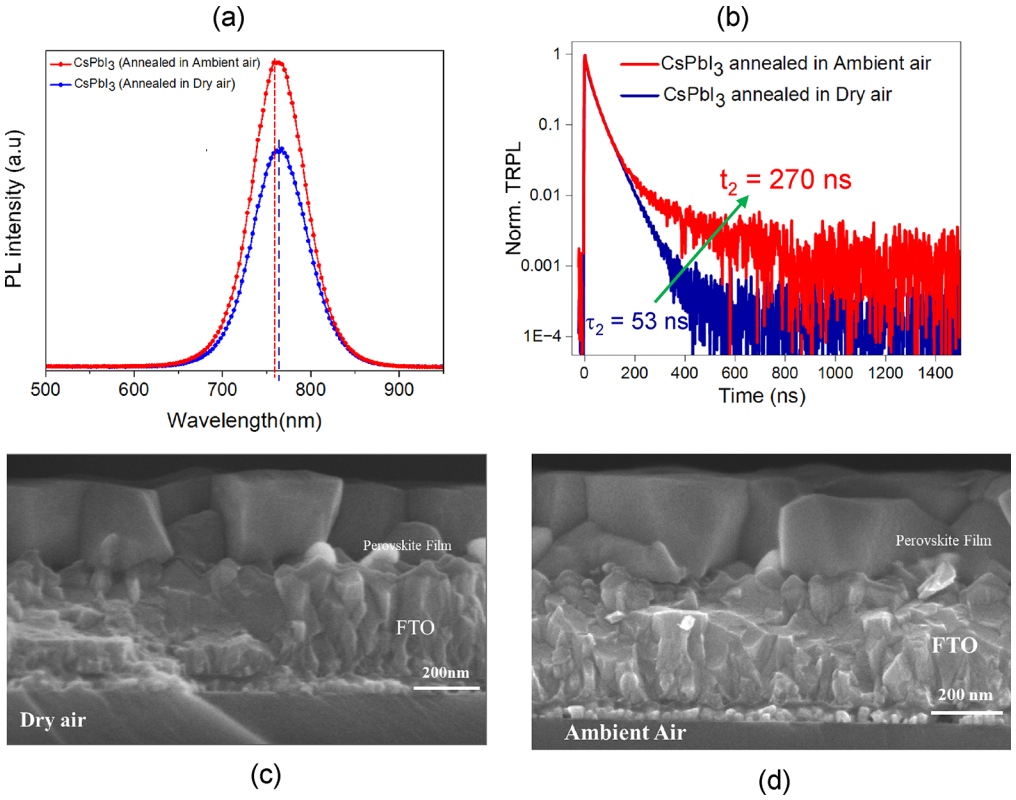

Figure 1. (a) Steady-state photoluminescence emission spectra of dry air and ambient air annealed $CsPbI_3$ absorbers. (b) Time-resolved photoluminescence (TRPL) decay of dry air and ambient air annealed $CsPbI_3$ films (fitted spectra are shown in Figure S4a,b). Cross-sectional SEM images of dry air (c) and ambient air, (d) annealed $CsPbI_3$ absorber films were deposited on FTO/TiO_2−C substrates.

DMAI sublimes in dry air while controlling the crystallization kinetics of $CsPbI_3$ films.[36] Generally, the absorber for perovskite solar cells is annealed in the glovebox (with a controlled environment) or dry air box (with oxygen contents). These controlled environments significantly increase the operational costs for industrial processes, so ambient environment annealing will be cost-effective.[37] The necessity of annealing in a dry airbox instead of a nitrogen-filled glovebox was also investigated.[38,39] It is found that annealing in the presence of oxygen removes the organic cations in the precursor solution and passivates halide vacancies, resulting in a higher open circuit voltage (V_{OC}).[40]

For all-inorganic perovskite-based devices, the open circuit voltage deficit (V_{loss}) is higher than that in all corresponding compositions of organic−inorganic halide perovskite solar cells.[41,42] Thus, the record V_{OC} of devices based on $CsPbI_3$ is still limited to ∼1.25 V.[43−45] The V_{OC} of the solar cells depends on the interfacial physical properties.[46−51] Until today, there has existed an information gap for $CsPbI_3$-based solar cells, such as the effect of the annealing environment on the surface chemistry, its subsequent interface, and charge extraction dynamics, which have been suggested to be the main V_{OC} bottlenecks.[52] We have used a state-of-the-art method for $CsPbI_3$ film preparation and device fabrication[53] in our study to address the mentioned knowledge gap.

In this work, we report a detailed analysis of the interface between $CsPbI_3$ and the hole transport material (HTM) and how its properties are affected by annealing in ambient air and a dry air box. We conducted steady-state photoluminescence spectroscopy (stPL) and time-resolved photoluminescence spectroscopy (TRPL) to determine the emission and charge carrier lifetimes. In addition, transient surface photovoltage (trSPV) measurements were conducted to investigate charge carrier extraction at the interface. At the same time, hard X-ray photoelectron spectroscopy (HAXPES) was used to probe the chemical and electronic structure of the differently annealed $CsPbI_3$ and perovskite/hole transport layer interface. Finally, we fabricated $CsPbI_3$-based devices. Using ambient air-annealed absorbers, PCE values of up to 19.8% have been reached (representing an improvement of >1% on an absolute scale compared to cells based on dry air-annealed absorbers). This improvement is mainly due to a systematic V_{OC} gain, reaching values up to 1.23 V, demonstrating that the annealing of $CsPbI_3$ films in ambient air is economically beneficial. Hence, this work not only paves the way for new fabrication strategies involving ambient air annealing processing but also contributes to solving the main challenge of V_{OC} deficit (V_{loss}) with a reduction of ∼ 0.47 V.

2. RESULTS AND DISCUSSION

2.1. Film Characterization. In recent work on $CsPbI_3$, researchers are using DMAI as a precursor along with PbI_2 and CsI. This organic molecule (DMAI) sublimes at ∼90 °C during annealing in dry air-box conditions with controlled humidity.[36] The annealing step/environment plays a vital role in the crystallization and growth and, thus, the overall quality of the absorber material.[54−57] Here, we report the impact of two different annealing processes on the properties of $CsPbI_3$: One approach is based on annealing in a dry air box with relative humidity (RH) controlled to be at ∼1% (hereafter, referred to as "dry air"), and the other process takes place in ambient air with RH between ∼45 to 50% (hereafter, referred

https://doi.org/10.1021/jacs.3c11711
J. Am. Chem. Soc. 2024, 146, 4642−4651

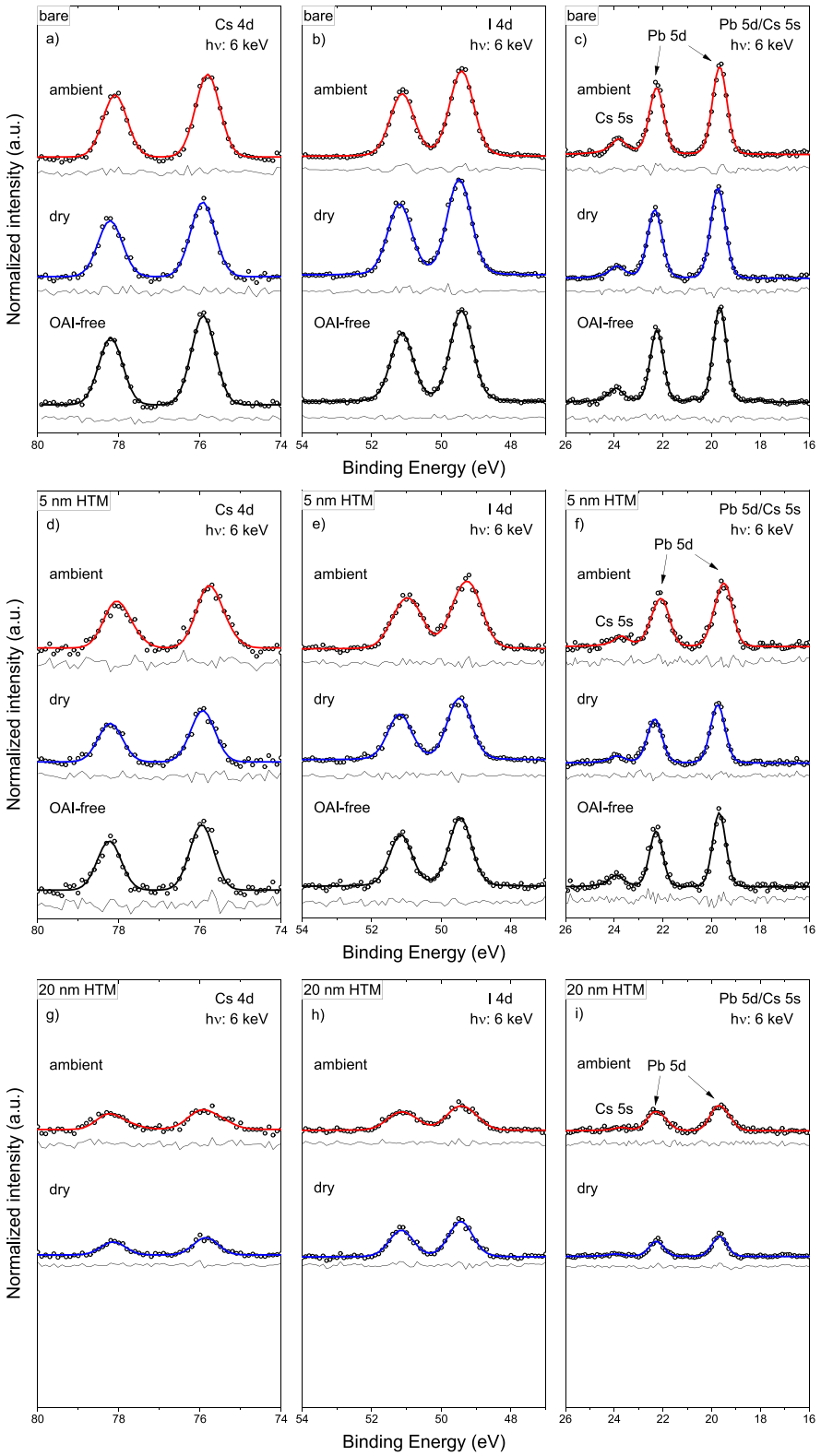

Figure 2. HAXPES detail spectra of the Cs 4d (a, d, g), I 4d (b, e, h), and overlapping Pb 5d/Cs 5s (c, f, i) photoemission lines for the variously treated $CsPbI_3$ films (i.e., OAI-free, dry air, and ambient air annealed) with 0 nm (i.e., bare) (a, b, c), 5 nm (d, e, f), and 20 nm (g, h, i) films of spiro-OMeTAD, respectively. The spectra were measured using 6 keV excitation and normalized to background intensity, with vertical offsets added for clarity. Curve fit results are included.

to as "ambient air"). These absorbers were subsequently capped with a 10−20 nm layer of *n*-octylammonium iodide (*n*-OAI) with a 2D structure, improving their stability.[53,58] As a reference, we also study dry air-annealed $CsPbI_3$ absorbers without *n*-OAI (hereafter, referred to as "OAI-free").

Initial characterization of the absorbers with ultraviolet−visible (UV−vis) absorption spectroscopy (Figure S1) shows

https://doi.org/10.1021/jacs.3c11711
J. Am. Chem. Soc. 2024, 146, 4642−4651

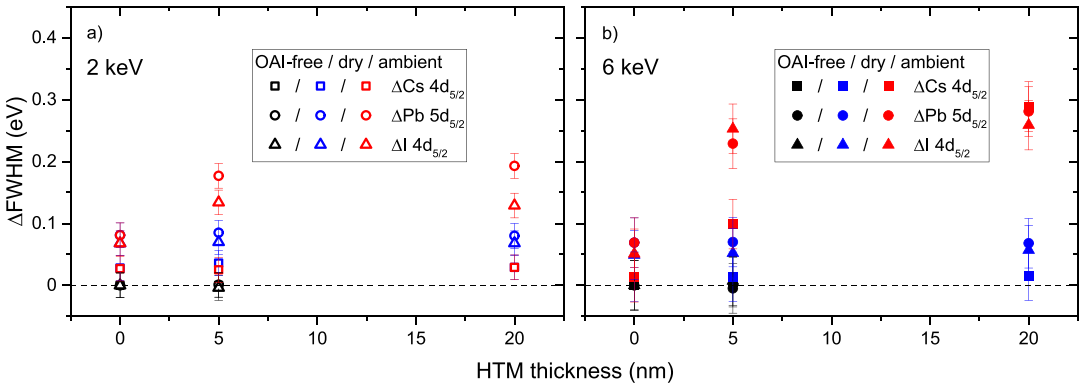

Figure 3. Changes in full-width-half-maximum (FHWM) values of the HAXPES Cs $4d_{5/2}$, Pb $5d_{5/2}$, I $4d_{5/2}$ peaks of $CsPbI_3$ absorbers annealed in dry or ambient air with 0 nm (i.e., bare), 5 and 20 nm films of HTM, measured with excitation energies of (a) 2 and (b) 6 keV (derived from the spectra shown in Figures S8 and 2), compared to the corresponding peak FHWM values of the bare, OAI-free $CsPbI_3$ sample.

that both dry air and ambient air-annealed $CsPbI_3$ films have an absorption edge at around 735 nm, indicating E_g values of ∼1.69 eV (see Tauc plots of UV−vis spectra in Figure S2), which is inconsistent with the E_g values (1.69−1.71 eV) for $CsPbI_3$ available in the literature.[36,42,53] Steady-state photoluminescence (stPL) emission spectroscopy was conducted using an excitation light with a wavelength of 445 nm on the top side of the film (perovskite side). The excitation wavelength and illumination direction are important in PL analysis to know the penetrations and surface passivation.[59] stPL reveals a PL peak emission at 764 nm for the dry air-annealed $CsPbI_3$, while for the ambient air-annealed $CsPbI_3$, the PL peak is slightly blue-shifted to 762 nm (see Figure 1a). The higher PL intensity and blue shift in the excitation peak indicate defect passivation on the surface of the ambient air-annealed $CsPbI_3$ film.[39,59−61] TRPL spectra measured on Glass/TiO_2/$CsPbI_3$: OAI dry air and ambient air annealed samples, given in Figure 1b, were fitted with the biexponential eq S8. The fitted parameters for the TRPL spectra are presented in Figure S3a,b and values in Table S1. We attribute the initial exponential decay (t_1) to charge transfer to TiO_2 and the second exponential decay (t_2) to nonradiative interfacial recombination.[33,62] Overall, TRPL is consistent with the stPL measurements and confirms that air-annealed samples have comparatively fewer defects.[33,35,36,60] Furthermore, we analyzed the morphology of the annealed $CsPbI_3$ films. Figure 1c,d shows the cross-sectional scanning electron microscopy (SEM) images for the dry air and ambient air annealed absorbers, which show both films have similar thicknesses (∼350 nm). Top-view SEM images confirm this (see Supporting Information, SI, Figure S4a,b), which show that the $CsPbI_3$ films exhibit similar compact, smooth, and pinhole-free morphologies, with similar grain sizes, i.e., ∼500 nm. The SEM images also show the absence of "fuzzy" grains previously attributed to remainders of unreacted precursors (e.g., DMAI).[36]

2.2. Surface Chemistry and Electronic Structure Profile Investigation by HAXPES. The surface and interface chemical modifications induced by two different annealing atmospheres were characterized by using HAXPES. For this purpose, the $CsPbI_3$ samples were deposited on F-doped tin oxide (FTO) coated glass substrates, a transparent conducting oxide material used in solar cell devices. Besides the bare $CsPbI_3$ absorber samples, we have made a series of additional HTM/$CsPbI_3$ samples also to study the interface properties, i.e., on the dry air annealed with an OAI-free as well as on the dry air and ambient air annealed $CsPbI_3$ absorbers with *n*-OAI passivation, spiro-OMeTAD based HTM layers of different (nominal) thicknesses of 0 nm (bare), 5, 20, and 200 nm were deposited. HAXPES survey spectra of the bare samples in Figure S5a confirm the presence of all expected elements: Cs, Pb, and I-related photoemission signals were observed in all samples, and C and N-related photoemission signals were observed only in the OAI-treated samples. Contrarily to previous reports that terminal ions make bonds with oxygen at the surface,[39] no visible contamination by e.g., oxygen is seen to result from the annealing treatments in different RH, and close examination of the most prominent halide perovskite-related HAXPES peaks, Cs 3d, I 3d, and Pb 4f (Figures S6 and S7) and the corresponding shallow core level peaks, Cs 4d, I 4d, and Pb 5d (Figures 2 and S8) show no significant change in line shape between the measurements of the dry air and ambient air annealed (and *n*-OAI passivated) $CsPbI_3$ absorbers. However, the corresponding photoemission lines of the OAI-free $CsPbI_3$ seem to be systematically narrower, which is attributed to the formation of an *n*-OAI-modified thin surface layer (with slightly different chemical and electronic structure compared to that of the OAI-free $CsPbI_3$ absorber). Furthermore, the OAI-free $CsPbI_3$ absorber also exhibits a small signal from metallic Pb, which is absent in the *n*-OAI treated samples, an effect most easily detected in Figures S6c and S8c. The survey spectra of the HTM thickness series in Figure S5b−d are consistent with the growth of a spiro-OMeTAD-based HTM (now also exhibiting F and S-related HAXPES contributions from LiTSFI and FK 209, which are included in the HTM-mixture, see discussion in SI), which increasingly attenuates the photoemission signal from the underlying $CsPbI_3$ as it becomes thicker, with only HTM-related signals appearing for the sample with a 200 nm thick HTM. There is little or no difference in the growth and composition of the HTM layer on the differently prepared $CsPbI_3$ films, except for the 5 nm data set, where a clear F 1s signal is present only in the spectrum measured on the sample prepared with an OAI-free $CsPbI_3$. Quantification of the Cs:Pb:I stoichiometry for the 0, 5, and 20 nm (shown in Figure S9a,b based on the measurements of perovskite-related shallow core levels using 2 and 6 keV, respectively; for more details, see the experimental section in the SI) confirms that the elemental composition is unchanged as a result of either the different annealing processes or by the deposition of the

https://doi.org/10.1021/jacs.3c11711
J. Am. Chem. Soc. 2024, 146, 4642−4651

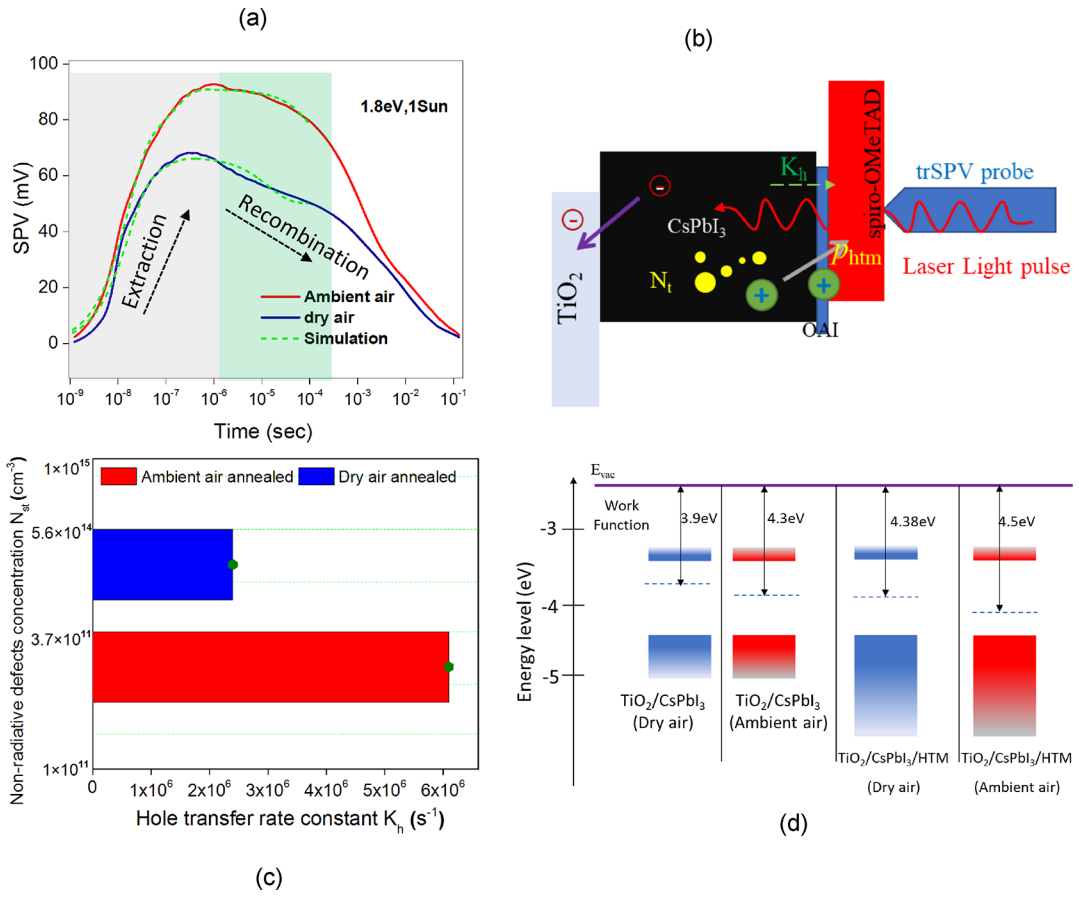

Figure 4. Interfacial dynamics. (a) Surface photovoltage (SPV) measurements for ETM/$CsPbI_3$/HTM samples based on absorbers annealed in dry and ambient air. The samples were measured under 1 sun illumination and using 1.8 eV laser excitation and recorded in ambient air conditions. The extracted hole concentrations p_{htm} induce the simulated trSPV signal, shown by green curves. (b) Charge extraction and recombination model describing carrier transport to the HTM layer. The constant K_h corresponds to hole injection rates from the perovskite to the HTM side. Defect concentration N_t is responsible for Shockley-Read-Hall recombination (SRH) of nonradiative recombination. (c) K_h and nonradiative defect concentration N_{st} values were extracted from the fitting. (d) Work function measurements with the Kelvin Probe method for dry air-annealed and ambient air-annealed samples.

HTM, with the most significant differences being the slightly elevated I and decreased Pb photoemission line intensities associated with the presence of the OAI-modified surface layer. This stability of the $CsPbI_3$ composition and its good agreement with the nominal composition suggest that no extensive chemical reactions have occurred at the surface of the bare $CsPbI_3$ absorbers or the corresponding interfaces to the HTM.

Despite this apparent chemical stability, close inspection of the collected HAXPES HTM/$CsPbI_3$ data reveals that there is a slight change in the line widths of the perovskite-derived core level spectra between the dry air and ambient air annealed $CsPbI_3$ absorbers: the photoemission lines collected for the samples based on $CsPbI_3$ absorbers annealed in ambient air are slightly broader in all cases, as presented in Figure 3a,b. Such a broadening can arise from changes in chemical structure (i.e., formation of new species beneath the HTM) or electronic structure profiles. Due to the relatively high information depth of HAXPES measurements, probing a sample volume in which band bending occurs may result in a line broadening[63−66] rather than or in addition to a shift in peak position. As discussed above, we do not see any indications of pronounced chemical changes in the $CsPbI_3$ films. However, because of the same high HAXPES information depth-induced integration effect, the formation of a thin interlayer (similar to the differences we observe due to the occurrence of OAI-induced surface modification) cannot be ruled out. In the case that one would attribute the observed line broadening to be due to a band bending enhancement, one could speculate that the ambient air annealing alters the defect distribution and concentration in the $CsPbI_3$ absorber, allowing for a more pronounced upward band bending in the absorber upon interface formation with the HTM. An interface-formation-induced upward band bending in the absorber, i.e., a binding energy (BE) shift of the absorber-related photoemission lines toward the Fermi-level (reducing the binding energy) can indeed be observed when comparing the halide perovskite-related photoemission lines for the HTM/$CsPbI_3$ samples based on absorbers annealed in ambient and dry air. The BE of the Cs 3d, I 3d, and Pb 4f (Figures S6 and S7) lines and of the corresponding shallow core level peaks Cs 4d, I 4d, and Pb 5d (Figures 2 and S8) of the HTM/$CsPbI_3$ samples based on the absorber annealed in ambient air are systematically lower than those made from absorbers annealed in dry air. (Shifts in BE of the peaks Cs $4d_{5/2}$, I $4d_{5/2}$, and Pb $5d_{5/2}$ peaks of the investigated samples compared to BE values of the bare, OAI-free $CsPbI_3$ sample are presented in Figure S9c,d.) This effect is most pronounced for the samples with a nominal 5 nm thick

https://doi.org/10.1021/jacs.3c11711
J. Am. Chem. Soc. 2024, 146, 4642−4651

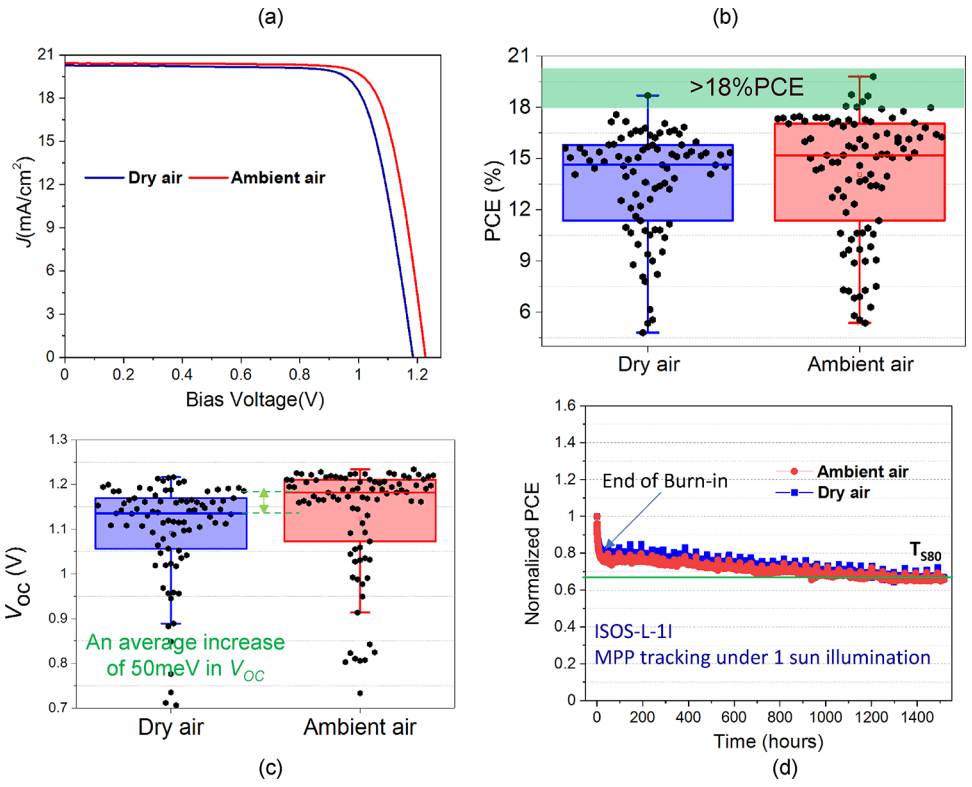

Figure 5. (a) $J-V$ curve for champion dry air and ambient air annealed $CsPbI_3$ film-based devices. Box chart statistics of 18 dry air and 18 ambient air annealed film-based individual devices with a total of over 90 pixels showing corresponding. (b) PCE and (c) V_{OC} values. (d) Long-term stability measurements for 1500 h for dry and ambient air-annealed $CsPbI_3$ film-based devices.

HTM layer, while we do not see for the HTM/$CsPbI_3$ samples with a nominal 20 nm Spiro-OMeTAD film.

2.3. Charge Carrier Extraction Dynamics and Trap Passivation. We further investigated the change in interface dynamics induced by the annealing medium. Charge carrier extraction by hole transport layer (HTL) and electron transport layer (ETL) is essential to PSC. The hole extraction rate coefficient (K_h) determines how fast holes can be extracted from the active perovskite absorber to the selective HTL layer. The knowledge of K_h for different HTL interfaces allows them to cross-compare their hole extraction capabilities.[62] The fast extraction—$1/K_h$ < carrier lifetime—ensures the collection of the carriers before their recombination in the active material or surface.[67,68] Further, transient surface photovoltage (trSPV) measurements were conducted to study charge carrier extraction dynamics for two devices (FTO/TiO_2/Perovskite: OAI/spiro-OMeTAD) annealed at different conditions (i.e., dry air and ambient air). To generate charge carriers, we used a 5 ns light pulse with a photon energy of 1.8 eV and fluence equal to 1 sun (more details in SI). The spectral dependence trSPV mapping is shown in Figure S11. The trSPV measurements revealed a significant boost in the amplitude and rise speed of the ambient air-annealed sample signal compared to the dry air-annealed sample, as shown in Figure 4a. The increase in the trSPV signal can be caused by more efficient charge extraction, larger K_h or suppressed trap concentration.[42,62,67,68] Another piece of evidence on more favorable band bending at the surface of the ambient air facilitating hole extraction comes from the Kelvin probe measurements as shown in Figure 4d, detailed in Figure S12, values added in Table S2. It is found that the work function increases from 3.88 eV for the dry air to 4.30 eV for the ambient air annealed sample, which is now much closer to that of the HTM layer. The change in work function (WF) is in line with the upward band bending inferred from the HAXPES data. Both trap passivation and favorable band bending can enhance the charge extraction at the HTL interface. To resolve two phenomena, we have applied charge carrier simulation based on the kinetic equation shown in our previous work[42] to access the charge carrier extraction rate constant and concentration of traps at the perovskite surface (Details and results of the simulation can be found in the SI and Tables S3 and S4.) After fitting experimental results, we found that the ambient air annealed sample has a three times faster charge carrier extraction rate, which resulted in the more rapid rise of the trSPV signal, as shown in Figure 4c. It shows that the air-annealed sample also exhibits a much lower concentration of defects (5.6×10^{11} cm^{-3} compared to 3.7×10^{14} cm^{-3} as derived for the dry air-annealed selection) at the perovskite surface, which may act as charge carrier recombination centers. The results suggest that air annealing enhances hole extraction and at the same time passivates defects, thereby improving charge carrier collection at the HTL interface.

2.4. Device Performance. We have used dry and ambient air annealed halide perovskite $CsPbI_3$ absorbers to fabricate $n-i-p$ devices with the structure: FTO/compact-TiO_2/$CsPbI_3$/OAI/spiro-OMeTAD/Au. After fabrication of the device, the device was stored in a dry air box to oxidize the spiro-OMeTAD layer. This oxidation induces changes in the lowest unoccupied molecular orbital (LUMO) levels of spiro-OMeTAD, making it more p-type.[69,70] However, the O_2-soaking duration required for reaching the highest device performance for ambient air and dry air annealed light absorbers differs, as shown in Figure S13. It shows that

https://doi.org/10.1021/jacs.3c11711
J. Am. Chem. Soc. 2024, 146, 4642−4651

devices based on halide perovskite absorbers annealed in dry air need longer oxygen soaking than cells based on $CsPbI_3$ annealed in ambient air. The underlying reason for this difference could be related to the enhanced band bending suggested for the samples annealed in ambient air, presumably establishing proper interface energetics without tuning the doping concentration of the HTM.

Figure 5a shows $J-V$ curves for the champion devices. The ambient-air annealed absorber device exhibits a PCE of 19.8%, a V_{OC} of 1.23 V, a current density (J_{SC}) of 20.4 mA/cm^{2,} and a fill factor (*FF*) of 78.9%, clearly outperforming the champion dry-air annealed device, reaching a PCE of 18.6%, a V_{OC} of 1.18 V, a J_{SC} of 20.2 mA/cm^2 and an *FF* of 77.76% (Table S5 and Figure S14). We have made 36 devices (18 for each absorber annealing condition), each containing 6 pixels (individual cells). The performance statistics are summarized in Figures 5b,c, and S15 and S16, corroborating a clear statistical difference between the cells based on differently annealed $CsPbI_3$ absorbers. For example, there is almost a 50 meV increase in V_{OC} for the devices based on the ambient-air annealed absorbers. Figure S17 shows the external quantum efficiency (EQE) measurements for the champion dry- and ambient-air annealed absorber devices. It shows an increase in EQE for the solar cell based on the ambient-air annealed $CsPbI_3$ in the wavelength range of 619−710 nm, which is attributed to a reduction in nonradiative recombination.[71] The J_{SC} calculated from EQE is 20.39 and 20.42 mA/cm^2 for devices based on dry-air and ambient-air annealed $CsPbI_3$, respectively. Finally, the long-term stability of both types of devices was measured for 1500 h. We have performed measurements of the devices at maximum power point (MPP tracking) under 1.2 sun illumination following ISOS-L-1I protocol.[72] Four devices for each condition were measured. Figure 5d shows the normalized PCE over time for 13,13 pixels for dry and ambient air-annealed sample devices. We can explain their stability in terms of T_{S80}. At the same time, T_{s80} is when there is a 20% drop in the PCE of the device after burn-in.[69,73] Both devices show similar stability with burn-in in the initial few hours dedicated to ion migration[74−76] and then similar T_{S80} values.

3. CONCLUSIONS

We have conducted a detailed surface and interfacial study for $CsPbI_3$ in perovskite solar cells and how they are impacted by the postpreparation annealing step in a dry air box and in an ambient air environment. We have found that the $CsPbI_3$ film annealed in ambient air has fewer defects, confirmed by PL and TRPL. A detailed HAXPES study of the surface and interface properties suggests an ambient-air-annealing-induced band bending enhancement at the $CsPbI_3$/HTM interface, presumably caused by the passivation of defect states. However, it confirms no chemical changes on the $CsPbI_3$ surface while annealing. By trSPV, we see improving charge carrier extraction and low nonradiative interfacial defects for air-annealed samples due to trap passivation and favorable surface band bending. The perovskite solar cells based on ambient air-annealed $CsPbI_3$ result in a PCE of 19.8%, a V_{OC} of 1.23 V, and T_{s80} up to 1500 h. This overall study opens the horizons for new annealing strategies and interfacial studies focusing on inorganic perovskite solar cells as a tool to reduce V_{loss}.

ASSOCIATED CONTENT

Supporting Information

The Supporting Information is available free of charge at https://pubs.acs.org/doi/10.1021/jacs.3c11711.

Detailed experimental method and device fabrication method; thin film characterization, UV−vis spectroscopy, SEM analysis, HAXPES survey spectra, and detailed analysis of the measurements; contour plots of the transient SPV, transient SPV fitting results, and simulation details; Kelvin probe measurements; champion $J-V$ of $CsPbI_3$ solar cells and EQE; and box charts of PCE, J_{sc}, V_{oc}, and *FF* (PDF)

AUTHOR INFORMATION

Corresponding Authors

Antonio Abate − *Helmholtz-Zentrum Berlin für Materialien und Energie GmbH, 14109 Berlin, Germany; Department of Chemistry, Bielefeld University, 33615 Bielefeld, Germany;* orcid.org/0000-0002-3012-3541; Email: antonio.abate@helmholtz-berlin.de, antonioabate83@gmail.com

Qiong Wang − *Helmholtz-Zentrum Berlin für Materialien und Energie GmbH, 14109 Berlin, Germany;* orcid.org/0000-0002-5849-4352; Email: qiong.wang@helmholtz-berlin.de

Authors

Zafar Iqbal − *Helmholtz-Zentrum Berlin für Materialien und Energie GmbH, 14109 Berlin, Germany;* orcid.org/0000-0003-0502-8136

Roberto Félix − *Helmholtz-Zentrum Berlin für Materialien und Energie GmbH, 14109 Berlin, Germany;* orcid.org/0000-0002-3620-9899

Artem Musiienko − *Helmholtz-Zentrum Berlin für Materialien und Energie GmbH, 14109 Berlin, Germany*

Jarla Thiesbrummel − *Institute for Physics and Astronomy, University of Potsdam, 14476 Potsdam-Golm, Germany; Clarendon Laboratory, University of Oxford, Oxford OX1 3PU, UK*

Hans Köbler − *Helmholtz-Zentrum Berlin für Materialien und Energie GmbH, 14109 Berlin, Germany*

Emilio Gutierrez-Partida − *Institute for Physics and Astronomy, University of Potsdam, 14476 Potsdam-Golm, Germany*

Thomas W. Gries − *Helmholtz-Zentrum Berlin für Materialien und Energie GmbH, 14109 Berlin, Germany*

Elif Hüsam − *Helmholtz-Zentrum Berlin für Materialien und Energie GmbH, 14109 Berlin, Germany*

Ahmed Saleh − *Helmholtz-Zentrum Berlin für Materialien und Energie GmbH, 14109 Berlin, Germany*

Regan G. Wilks − *Helmholtz-Zentrum Berlin für Materialien und Energie GmbH, 14109 Berlin, Germany; Energy Materials In-situ Laboratory Berlin (EMIL), Helmholtz-Zentrum Berlin für Materialien und Energie GmbH, 12489 Berlin, Germany;* orcid.org/0000-0001-5822-8399

Jiahuan Zhang − *Helmholtz-Zentrum Berlin für Materialien und Energie GmbH, 14109 Berlin, Germany*

Martin Stolterfoht − *Institute for Physics and Astronomy, University of Potsdam, 14476 Potsdam-Golm, Germany; Electronic Engineering Department, The Chinese University of Hong Kong, Hong Kong 999077, SAR China;* orcid.org/0000-0002-4023-2178

https://doi.org/10.1021/jacs.3c11711
J. Am. Chem. Soc. 2024, 146, 4642−4651

Dieter Neher − *Institute for Physics and Astronomy, University of Potsdam, 14476 Potsdam-Golm, Germany;* orcid.org/0000-0001-6618-8403

Steve Albrecht − *Helmholtz-Zentrum Berlin für Materialien und Energie GmbH, 14109 Berlin, Germany;* orcid.org/0000-0001-9962-9535

Marcus Bär − *Helmholtz-Zentrum Berlin für Materialien und Energie GmbH, 14109 Berlin, Germany; Department of Chemistry and Pharmacy, Friedrich-Alexander-Universität Erlangen-Nürnberg (FAU), 91058 Erlangen, Germany; Helmholtz Institute Erlangen-Nürnberg for Renewable Energy (HI ERN), 12489 Berlin, Germany; Energy Materials In-situ Laboratory Berlin (EMIL), Helmholtz-Zentrum Berlin für Materialien und Energie GmbH, 12489 Berlin, Germany;* orcid.org/0000-0001-8581-0691

Complete contact information is available at: https://pubs.acs.org/10.1021/jacs.3c11711

Author Contributions

All the authors have contributed to the draft's data explanation, writing, and proofreading.

Notes

The authors declare no competing financial interest.

■ ACKNOWLEDGMENTS

Z.I. is thankful to Deutscher Akademischer Austauschdienst (DAAD) for a Ph.D. scholarship to study at HZB. He also acknowledges the generous help of Mrs. Carola Klimm for the SEM characterization. A.M. acknowledges financial funding from the European Union HORIZON-MSCA-2021-PF-01-01 under grant agreement no. 101061809 (HyPerGreen). We thank HZB for the allocation of synchrotron radiation beamtime. We gratefully acknowledge Dr. Thomas Dittrich for providing the HZB SPV lab facilities. We acknowledge HyPerCells (a joint graduate school of the University of Potsdam and the Helmholtz-Zentrum Berlin) and the Deutsche Forschungsgemeinschaft (DFG, German Research Foundation) − project number 423749265 and 424709669 − SPP 2196 (SURPRISE-2, HIPSTER and HIPSTER-PRO) for funding. We also acknowledge financial support from the Federal Ministry for Economic Affairs and Energy within the framework of the seventh Energy Research Programme (P3T-HOPE, 03EE1017C). M.S. further acknowledges the Heisenberg program from the Deutsche Forschungsgemeinschaft (DFG, German Research Foundation) project number 498155101 as well as the Vice Chancellor Early Carrer Professorship Scheme from CUHK for funding.

■ REFERENCES

(1) Innocenzo, V. D.; Kandada, A. R. S.; Bastiani, M. D.; Gandini, M.; Petrozza, A. Tuning the Light Emission Properties by Band Gap Engineering in Hybrid Lead Halide Perovskite. *J. Am. Chem. Soc.* **2014**, *136*, 17730−17733.

(2) Kulkarni, S. A.; Baikie, T.; Boix, P. P.; Yantara, N.; Mathews, N.; Mhaisalkar, S. Band-gap tuning of lead halide perovskites using a sequential deposition process. *J. Mater. Chem. A* **2014**, *2*, 9221−9225.

(3) Unger, E. L.; Kegelmann, L.; Suchan, K.; Sörell, D.; Korte, L.; Albrecht, S. Roadmap and roadblocks for the band gap tunability of metal halide perovskites. *J. Mater. Chem. A* **2017**, *5*, 11401−11409.

(4) Rehman, W.; Milot, R. L.; Eperon, G. E.; Wehrenfennig, C.; Boland, J. L.; Snaith, H. J.; Johnston, M. B.; Herz, L. M. Charge-Carrier Dynamics and Mobilities in Formamidinium Lead Mixed-Halide Perovskites. *Adv. Mater.* **2015**, *27*, 7938−7944.

(5) Lim, J.; Maximilian, T.; Sakai, N.; Snaith, Henry J.; et al. Elucidating the long-range charge carrier mobility in metal halide perovskite thin films. *Energy Environ. Sci.* **2019**, *12*, 169−176.

(6) Huang, H.; Bodnarchuk, M. I.; Kershaw, S. V.; Kovalenko, M. V.; Rogach, A. L. Lead Halide Perovskite Nanocrystals in the Research Spotlight: Stability and Defect Tolerance. *ACS Energy Lett.* **2017**, *2*, 2071−2083.

(7) Caena, J. B.; Saliba, M.; Buonassisi, T.; Grätzel, M.; Abate, A.; Hagfeldt, A. Promises and challenges of perovskite solar cells. *Science* **2017**, *358*, 739−744.

(8) Zhang, W.; Eperon, G.; Snaith, H. Metal halide perovskites for energy applications. *Nat. Energy* **2016**, *1*, 16048.

(9) Wolf, S. D.; Holovsky, J.; Moon, S. J.; Löper, P.; Niesen, B.; Ledinsky, M.; Haug, F. J.; Yum, J. H.; Ballif, C. Organometallic Halide Perovskites: Sharp Optical Absorption Edge and Its Relation to Photovoltaic Performance. *J. Phys. Chem. Lett.* **2014**, *5*, 1035−1039.

(10) Kojima, A.; Teshima, K.; Shirai, Y.; Miyasaka, T. Organometal Halide Perovskites as Visible-Light Sensitizers for Photovoltaic Cells. *J. Am. Chem. Soc.* **2009**, *131*, 6050−6051.

(11) Best Research-Cell Efficiency Chart https://www.nrel.gov/pv/interactive-cell-efficiency.html. (Accessed on June 02, 2023.).

(12) Green, M. A.; Dunlop, E. D.; Siefer, G.; Yoshita, M.; Kopidakis, N.; Bothe, K.; et al. Solar cell efficiency tables (Version 61). *Progress in Photovoltaics: Research and Applications* **2023**, *31*, 3−16.

(13) Zhu, L.; Zhang, M.; Xu, J.; Li, C.; Yan, J.; Zhou, G.; et al. Single-junction organic solar cells with over 19% efficiency enabled by a refined double-fibril network morphology. *Nat. Mater.* **2022**, *21*, 656−663.

(14) Green, M. A.; Ho-Bailli, A. W. Y. Pushing to the Limit: Radiative Efficiencies of Recent Mainstream and Emerging Solar Cells. *ACS Energy Lett.* **2019**, *4*, 1639−1644.

(15) Sha, W.E. I.; Ren, X.; Chen, L.; Choy, W. C. H. The efficiency limit of $CH_3NH_3PbI_3$ perovskite solar cells. *Appl. Phys. Lett.* **2015**, *106*, 221104.

(16) https://www.lmpv.nl/db/ (Accessed on June 20, 2023.).

(17) Philippe, B.; Park, B. W.; Lindblad, R.; Oscarsson, J.; Ahmadi, S.; Johansson, E.M. J.; Rensmo, H. Chemical and Electronic Structure Characterization of Lead Halide Perovskites and Stability Behavior under Different Exposures—A Photoelectron Spectroscopy Investigation. *Chem. Mater.* **2015**, *27*, 1720−1731.

(18) Christians, J. A.; Herrera, P.A. M.; Kamat, P. V. Transformation of the Excited State and Photovoltaic Efficiency of $CH_3NH_3PbI_3$ Perovskite upon Controlled Exposure to Humidified Air. *J. Am. Chem. Soc.* **2015**, *137*, 1530−1538.

(19) Lu, Y. B.; Cong, W. Y.; Guan, C. B.; Sun, H.; Xin, Y.; Wang, K.; Song, S. Light enhanced moisture degradation of perovskite solar cell material $CH_3NH_3PbI_3$. *J. Mater. Chem. A* **2019**, *7*, 27469−27474.

(20) Faheem, M. B.; Faheem, M. B.; Bilawal Khan, C.; Feng, M. U.; Farooq, F.; Raziq, Y.; Xiao, Y. Li All-Inorganic Perovskite Solar Cells: Energetics, Key Challenges, and Strategies toward Commercialization. *ACS Energy Lett.* **2020**, *5*, 290−320.

(21) Meng, H.; Shao, Z.; Wang, L.; Li, Z.; Liu, R.; Fan, Y.; Cui, G.; Pang, S. Chemical Composition and Phase Evolution in DMAI-Derived Inorganic Perovskite Solar Cells. *ACS Energy Lett.* **2020**, *5*, 263−270.

(22) Yao, H.; Zhao, J.; Li, Z.; Ci, Z.; Jin, Z. Research and progress of black metastable phase $CsPbI_3$ solar cells. *Mater. Chem. Front.* **2021**, *5*, 1221−1235.

(23) Ahmad, W.; Khan, J.; Niu, G.; Tang, J. Inorganic $CsPbI_3$ Perovskite-Based Solar Cells: A Choice for a Tandem Device. *Sol. RRL* **2017**, *1*, No. 1700048.

(24) Zhao, X.; Liu, T.; Burlingame, Q. C.; Liu, T.; Holley, R.; Cheng, G.; et al. Accelerated aging of all-inorganic, interface-stabilized perovskite solar cells. *Science* **2022**, *377*, 307−310.

(25) Xiang, W.; Liu, S. F.; Tress, W. A review on the stability of inorganic metal halide perovskites: challenges and opportunities for stable solar cells. *Energy Environ. Sci.* **2021**, *14*, 2090−2113.

(26) Steele, J. A.; Jin, H.; Dovgaliuk, I.; Berger, R. F.; Braeckevelt, T.; et al. Thermal unequilibrium of strained black $CsPbI_3$ thin films. *Science.* **2019**, *365* (6454), 679−684.
(27) Swarnkar, A.; Marshall, A. R.; et al. Quantum dot−induced phase stabilization of α-CsPbI3 perovskite for high-efficiency photovoltaics. *Science* **2016**, *354* (6308), 92−95.
(28) Ke, W.; Spanopoulos, I.; Stoumpos, C. C.; Kanatzidis, M. G. Myths and reality of $HPbI_3$ in halide perovskite solar cells. *Nat. Commun.* **2018**, *9*, 4785.
(29) Bian, H.; Li, H. Z.; Zhou, F.; Xu, Y.; Zhang, H.; Wang, Q.; Ding, L. Unveiling the Effects of Hydrolysis-Derived DMAI/DMAPbIx Intermediate Compound on the Performance of $CsPbI_3$ Solar Cells. *Adv. Sci.* **2020**, *7*, No. 1902868.
(30) Chang, X.; Fang, J.; Fan, Y.; Luo, T.; Su, H.; Zhang, Y.; Lu, J.; Tsetseris, L.; Anthopoulos, T. D.; Liu, S. F.; Zhao, K. Printable $CsPbI_3$ Perovskite Solar Cells with PCE of 19% *via* an Additive Strategy. *Adv. Mater.* **2020**, *32*, No. 2001243.
(31) Tan, S.; Shi, J.; Yu, B.; Zhao, W.; Li, Y.; Li, Y.; Wu, H.; Luo, Y.; Li, D.; Meng, Q. Inorganic Ammonium Halide Additive Strategy for Highly Efficient and Stable $CsPbI_3$ Perovskite Solar Cells. *Adv. Funct. Mater.* **2021**, *31*, No. 2010813.
(32) Zhang, J.; Fang, Y.; Wen, J.; Liu, S. F. Molten-Salt-Assisted $CsPbI_3$ Perovskite Crystallization for Nearly 20%-Efficiency Solar Cells. *Adv. Mater.* **2021**, No. 2103770.
(33) Yu, B.; Shi, J.; Tan, S.; Cui, Y.; Zhao, W.; Wu, H.; Luo, Y.; Li, D.; Meng, Q. Efficient (>20%) and Stable All-Inorganic Cesium Lead Triiodide Solar Cell Enabled by Thiocyanate Molten Salts. *Angew. Chem., Int. Ed.* **2021**, *60*, 13436−13443.
(34) Qiu, J.; Zhou, Q.; Jia, D.; Wang, Y.; Li, S.; Zhang, X. Robust molecular-dipole-induced surface functionalization of inorganic perovskites for efficient solar cells. *J. Mater. Chem. A* **2022**, *10*, 1821.
(35) Wang, Y.; Dar, M. I.; Ono, L. K.; Zhang, T.; Kan, M.; Li, Y.; Zhang, L.; Wang, X.; Yang, Y.; Gao, X.; Qi, Y.; Grätzel, M.; Zhao, Y. Thermodynamically stabilized ß-CsPbI3−based perovskite solar cells with efficiencies > 18%. *Science* **2019**, *365*, 591−595.
(36) Wang, Y.; Liu, X.; Zhang, T.; Wang, X.; Kan, M.; Shi, J.; Zhao, Y. The Role of Dimethylammonium Iodide in CsPbI3 Perovskite Fabrication: Additive or Dopant? *Angew. Chem.* **2019**, *131*, 16844−16849.
(37) Raga, S. R.; Jung, M.-C.; Lee, M. V.; Leyden, M. R.; Kato, Y.; Qi, Y. Influence of Air Annealing on High Efficiency Planar Structure Perovskite Solar Cells. *J. Mater. Chem.* **2015**, *27*, 1597−1603.
(38) Marshall, A. R.; Sansom, H. C.; McCarthy, M. M.; Warby, J. H.; Ashton, O. J.; Wenger, B.; Snaith, H. J. Dimethylammonium: An A-Site Cation for Modifying $CsPbI_3$. *Sol. RRL* **2021**, *5*, No. 2000599.
(39) Liu, S. C.; Li, Z.; Yang, Y.; Wang, X.; Chen, Y.-X.; Xue, D.-J.; Hu, J.-S. Investigation of Oxygen Passivation for High-Performance All-Inorganic Perovskite Solar Cells. *J. Am. Chem. Soc.* **2019**, *141*, 18075−18082.
(40) Wang, K.; Gao, C.; Xu, Z.; Tian, Q.; Gu, X.; Zhang, L.; Zhang, S.; Zhao, K.; Liu, S. F. In-Situ Hot Oxygen Cleansing and Passivation for All-Inorganic Perovskite Solar Cells Deposited in Ambient to Breakthrough 19% Efficiency. *Adv. Funct. Mater.* **2021**, *31*, No. 2101568.
(41) Grischek, M.; Caprioglio, P.; Zhang, J.; Pena-Camargo, F.; Sveinbjörnsson, K.; Zu, F.; et al. Efficiency Potential and Voltage Loss of Inorganic $CsPbI_2Br$ Perovskite Solar Cells. *Sol. RRL* **2022**, *6*, No. 2200690.
(42) Iqbal, Z.; Zu, F.; Musiienko, A.; Gutierrez-Partida, E.; Köbler, H.; Gries, T. W.; et al. Interface Modification for Energy Level Alignment and Charge Extraction in $CsPbI_3$ Perovskite Solar Cells. *ACS Energy Lett.* **2023**, *8*, 4304−4314.
(43) Mali, S. S.; Patil, J. V.; Shao, J.-Y.; Zhong, Y.-W.; Rondiya, S. R.; Dzade, N. Y.; et al. Phase-heterojunction all-inorganic perovskite solar cells surpassing 21.5% efficiency. *Nat. Energy* **2023**, *8*, 989−100.
(44) Cui, Y.; Shi, J.; Meng, F.; Yu, B.; Tan, S.; He, S.; Tan, C.; Li, Y.; Wu, H.; Luo, Y.; Li, D.; Meng, Q. A Versatile Molten-Salt Induction Strategy to Achieve Efficient $CsPbI_3$ Perovskite Solar Cells with a High Open-Circuit Voltage > 1.2 V. *Adv. Mater.* **2022**, *34*, No. 2205028.
(45) Liu, Y.; Xu, T.; Xu, Z.; Zhang, H.; Yang, T.; Wang, Z.; et al. Defect Passivation and Lithium Ion Coordination Via Hole Transporting Layer Modification for High Performance Inorganic Perovskite Solar Cells. *Adv. Mater.* **2023**, No. 2306982.
(46) Tress, W.; Yavari, M.; Domanski, K.; Yadav, P.; Niesen, B.; Correa Baena, J. P.; et al. Interpretation and evolution of open-circuit voltage, recombination, ideality factor and subgap defect states during reversible light-soaking and irreversible degradation of perovskite solar cells. *Energy Environ. Sci.* **2018**, *11*, 151−165.
(47) Pan, H.; Shao, H.; Zhang, X. L.; Shen, Y.; Wang, M. Interface engineering for high-efficiency perovskite solar cells. *J. Appl. Phys.* **2021**, *129*, 130904.
(48) Sandberg, O. J.; Sundqvist, A.; Nyman, M.; Österbacka, R. Relating Charge Transport, Contact Properties, and Recombination to Open-Circuit Voltage in Sandwich-Type Thin-Film Solar Cells. *Phys. Rev. Appl.* **2016**, *5*, No. 044005.
(49) Guo, Z.; Jena, A. K.; Kim, G. M.; Miyasaka, T. The high open-circuit voltage of perovskite solar cells: a review. *Energy Environ. Sci.* **2022**, *15*, 3171.
(50) Stolterfoht, M.; Grischek, M.; Caprioglio, P.; Wolff, C. M.; Gutierrez-Partida, E.; Camargo, F. P.; et al. How to Quantify the Efficiency Potential of Neat Perovskite Films: Perovskite Semiconductors with an Implied Efficiency Exceeding 28%. *Adv. Mater.* **2020**, *32*, No. 2000080.
(51) Stolterfoht, M.; Neher, D.; et al. The impact of energy alignment and interfacial recombination on the internal and external open-circuit voltage of perovskite solar cells. *Energy Environ. Sci.* **2019**, *12*, 2778.
(52) Xiang, W.; Liu, S. F.; Tress, W. Interfaces and Interfacial layers in Inorganic Perovskite Solar Cells. *Angew. Chem.* **2021**, *133*, 26644−26657.
(53) Yoon, S. M.; Min, H.; Kim, J. B.; Kim, G.; Lee, K. S.; Seok, S. Surface Engineering of Ambient-Air-Processed Cesium Lead Triiodide Layers for Efficient Solar Cells. *Joule* **2021**, *5*, 183−196.
(54) Chen, L.-C.; Chen, C.-C.; Chen, J.-C.; Wu, C.-G. Annealing effects on high-performance CH3NH3PbI3 perovskite solar cells prepared by solution-process. *Sol. Energy* **2015**, *122*, 1047−1051.
(55) Wang, C.; Zhao, Y.; Ma, T.; An, Y.; He, R.; Zhu, J.; et al. Universal close-space annealing strategy towards high-quality perovskite absorbers enabling efficient all-perovskite tandem solar cells. *Nat. Energy* **2022**, *7*, 744−753.
(56) Liu, K.; Luo, Y.; Jin, Y.; Liu, T.; Liang, Y.; Yang, L.; et al. Moisture-triggered fast crystallization enables efficient and stable perovskite solar cells. *Nat. Commun.* **2022**, *13*, 4891.
(57) Wang, H.; Liu, H.; Dong, Z.; Wei, X.; Li, W.; Zhu, L.; et al. Moisture is not always bad: H_2O accelerates the conversion of DMAPbI3 intermediate to $CsPbI_3$ for boosting the efficiency of carbon-based perovskite solar cells to over 16%. *Fundam. Res.* **2022**, DOI: 10.1016/j.fmre.2022.07.005.
(58) Kim, H.; Lee, S.-U.; Lee, D. Y.; et al. Optimal Interfacial Engineering with Different Length of Alkylammonium Halide for Efficient and Stable Perovskite Solar Cells. *Adv. Energy Mater.* **2019**, *9*, No. 1902740.
(59) Tian, Y.; Peter, M.; Unger, E.; Abdellah, M.; Zheng, K.; Pullerits, T.; et al. Mechanistic insights into perovskite photoluminescence enhancement: light curing with oxygen can boost yield thousandfold. *Phys. Chem. Chem. Phys.* **2015**, *17*, 24978−24987.
(60) Gu, X.; Xiang, W.; Tian, Q.; Liu, S. F. Rational Surface-Defect Control *via* Designed Passivation for High-Efficiency Inorganic Perovskite Solar Cells. *Angew. Chem.* **2021**, *133*, 23348−23354.
(61) Phung, N.; Mattoni, A.; Smith, J. A.; Skroblin, D.; Köbler, H.; et al. Photoprotection in metal halide perovskites by ionic defect formation. *Joule* **2022**, *6*, 2152−2174.
(62) Levine, I.; Al Ashouri, A.; Musiienko, A.; et al. Charge transfer rates and electron trapping at buried interfaces of perovskite solar cell. *Joule* **2021**, *5*, 2915−2933.

(63) Wippler, D.; Wilks, R. G.; Pieters, B. E.; Van Albada, S. J.; Gerlach, D.; Hüpkes, J. R.; et al. Pronounced surface band bending of thin-film silicon revealed by modeling core levels probed with hard x-rays. *ACS Appl. Mater. Interfaces* **2016**, *8*, 17685−17693.
(64) Romanyuk, O.; Paszuk, A.; Bartoš, I.; Wilks, R. G.; Nandy, M.; Bombsch, J.; et al. Band bending at heterovalent interfaces: Hard X-ray photoelectron spectroscopy of GaP/Si(0 0 1) heterostructures. *Appl. Surf. Sci.* **2021**, *565*, No. 150514.
(65) Romanyuk, O.; Supplie, O.; Paszuk, A.; Stoeckmann, J. P.; Wilks, R. G.; Bombsch, J.; et al. Hard X-ray photoelectron spectroscopy study of core level shifts at buried GaP/Si(001) interfaces. *Surf. Interface Anal.* **2020**, *52*, 933−938.
(66) Romanyuk, O.; Paszuk, A.; Gordeev, I.; Wilks, R. G.; Ueda, S.; Hartmann, C.; et al. Combining advanced photoelectron spectroscopy approaches to analyse deeply buried GaP(As)/Si(100) interfaces: Interfacial chemical states and complete band energy diagrams. *Appl. Surf. Sci.* **2022**, *605*, No. 154630.
(67) Musiienko, A.; Ceratti, D. R.; Pipek, J.; et al. Defects in Hybrid Perovskites: The Secret of Efficient Charge Transport. *Adv. Funct. Mater.* **2021**, *31*, No. 2104467.
(68) Fengler, S.; Kriegel, H.; Schieda, M.; et al. Charge Transfer in c-Si (n++)/TiO2 (ALD) at the Amorphous/Anatase Transition: A Transient Surface Photovoltage Spectroscopy Study. *ACS Appl. Mater. Interfaces* **2020**, *12*, 3140−3149.
(69) Hawash, Z.; Ono, L. K.; Raga, S. R.; Lee, M. V.; Qi, Y. Air-Exposure Induced Dopant Redistribution and Energy Level Shifts in Spin-Coated Spiro-MeOTAD Films. *Chem. Mater.* **2015**, *27*, 562−569.
(70) Abate, A.; Leijtens, T.; Pathak, S.; Teuscher, J.; Avolio, R.; Errico, M. E.; Kirkpatrik, J.; Ball, J. M.; Docampo, P.; McPherson, I.; Snaith, H. J. Lithium salts as "redox active" p-type dopants for organic semiconductors and their impact in solid-statedye-sensitized solar cells. *Phys. Chem. Chem. Phys.* **2013**, *15*, 2572.
(71) Han, Q.; Ding, J.; Bai, Y.; Li, T.; Ma, J.-Y.; Chen, Y.-X.; Zhou, Y.; Liu, J. Ge; et al. Carrier Dynamics Engineering for High-Performance Electron-Transport-Layer-free Perovskite Photovoltaics. *Chem.* **2018**, *4*, 2405.
(72) Khenkin, M. V.; Katz, E. A.; Abate, A.; et al. Consensus statement for stability assessment and reporting for perovskite photovoltaics based on ISOS procedures. *Nat. Energy* **2020**, *5*, 35−49.
(73) Rakocevic, L.; Ernst, F.; Yimga, N. T.; et al. Reliable Performance Comparison of Perovskite Solar Cells Using Optimized Maximum Power Point Tracking. *Sol. RRL* **2019**, *3*, No. 1800287.
(74) Kanda, H.; Shibayama, N.; Huckaba, A. J.; et al. Band-bending induced passivation: high performance and stable perovskite solar cells using a perhydropoly(silazane) precursor. *Energy Environ. Sci.* **2020**, *13*, 1222.
(75) Li, Q.; Zhao, Y.; Fu, R.; Zhou, W.; Zhao, Y.; Lin, F.; et al. Enhanced long-term stability of perovskite solar cells using a double-layer hole transport material. *J. Mater. Chem. A* **2017**, *5*, 14881−14886.
(76) Cristina, B.; Laura Elena, A.; Viorica, S.; et al. Iodine Migration and Degradation of Perovskite Solar Cells Enhanced by Metallic Electrodes. *J. Phys. Chem. Lett.* **2016**, *7*, 5168−5175.

https://doi.org/10.1021/jacs.3c11711
J. Am. Chem. Soc. 2024, 146, 4642−4651